Okhotsk Sea Kashevarov Bank polynya: Its dependence on diurnal and fortnightly tides and its initial formation

Seelye Martin,[1] Igor Polyakov,[2] Thorsten Markus,[3] and Robert Drucker[1]

Received 19 November 2003; revised 24 May 2004; accepted 24 June 2004; published 18 September 2004.

[1] A powerful resonance in the O1 and K1 diurnal tides occurs over the Kashevarov Bank in the Okhotsk Sea. Model studies show that this resonance creates tidal mixing and an associated vertical heat flux, both with diurnal and fortnightly components. In midwinter this flux controls the behavior of the resultant polynya; in early winter it affects the polynya formation. For the midwinter case, examination of numerical results and of imagery derived from the Special Sensor Microwave Imager (SSM/I), the advanced very high resolution radiometer (AVHRR), and the RADARSAT ScanSAR shows that the polynya area varies diurnally and fortnightly. Specifically, for the 2000 and 2001 winters, daily averaged passive microwave images clearly show a fortnightly cycle in the polynya area. At the diurnal period the model shows that the location of the maximum heat flux oscillates between the northwestern and southwestern edge of the bank and that the polynya oscillates between the western edge of the bank and being elongated in the east-west direction over the southern edge. Passive microwave swath and AVHRR imagery show a similar polynya behavior. For the early winter case and during a period of northerly winds, synthetic aperture radar imagery shows that the polynya consists of two parts, an upwelling polynya over the bank and a secondary polynya downwind of the bank with properties similar to coastal polynyas. In the case of the secondary polynya the region of upwelled warm water over the bank serves as its northern boundary. *INDEX TERMS:* 4540 Oceanography: Physical: Ice mechanics and air/sea/ice exchange processes; 4275 Oceanography: General: Remote sensing and electromagnetic processes (0689); 4243 Oceanography: General: Marginal and semienclosed seas; 4207 Oceanography: General: Arctic and Antarctic oceanography; *KEYWORDS:* Kashevarov Bank, Okhotsk Sea, polynyas

Citation: Martin, S., I. Polyakov, T. Markus, and R. Drucker (2004), Okhotsk Sea Kashevarov Bank polynya: Its dependence on diurnal and fortnightly tides and its initial formation, *J. Geophys. Res.*, *109*, C09S04, doi:10.1029/2003JC002215.

1. Introduction

[2] It has been long recognized that the polynya that forms over the Kashevarov Bank in the Okhotsk Sea is due to a tidal resonance [*Alfultis and Martin*, 1987; *Polyakov and Martin*, 2000]. *Kowalik and Polyakov* [1998] discuss the nature of the Okhotsk tides and the tidal resonance over the bank. *Polyakov and Martin* [2000] discuss the diurnal and fortnightly dependence of the heat flux and show that it is a maximum over the bank and in particular, over its western rise. From mooring observations, *Rogachev et al.* [2001] show that over the bank, the observed tidal mixing varies with the fortnightly tide. They also present winter advanced very high resolution radiometer (AVHRR) imagery that suggests a fortnightly fluctuation in the polynya size.

[3] Figures 1a and 1b, respectively, show charts of the Okhotsk Sea and the details of the Kashevarov Bank topography. Figure 1a combines two topographies derived from Russian navigational charts. The overall Okhotsk Sea chart is a 5′ digitized version of a topographic chart with a 1:2,000,000 scale. This topography is used by *Kowalik and Polyakov* [1998] and by *Polyakov and Martin* [2000]. The specific Kashevarov topography used in both figures is taken from a Russian navigation chart with a much higher resolution, approximately 1:100,000 or 1 cm: 5 km, with an accuracy of about 1 km. It was digitized by our Russian colleagues from the Arctic and Antarctic Research Institute. Figure 1b shows the bank topography, where the 200-m contour is assumed to outline the bank. The figure shows that the longitudinal axis of the bank is oriented east-west, and that the bank is highest to the west, where it rises to a depth of 105 m. The black dot at the western bank summit will be referred to in our heat flux discussion.

[4] The paper divides into seven parts. Section 2 describes our numerical model and shows that the heat flux over the bank has a fortnightly and diurnal component. Section 3 compares a RADARSAT ScanSAR image with a

[1]School of Oceanography, University of Washington, Seattle, Washington, USA.
[2]International Arctic Research Center, University of Alaska Fairbanks, Fairbanks, Alaska, USA.
[3]Laboratory for Hydrospheric Processes, NASA Goddard Space Flight Center, Greenbelt, Maryland, USA.

0148-0227/04/2003JC002215$09.00

Figure 1a. Okhotsk Sea bathymetry.

nearly simultaneous AVHRR image taken during a period when the polynya is open, and shows that the radar backscatter is consistent with the polynya being made up of a mixture of ice floes and open water. Section 4 shows from daily averaged passive microwave data for the years 2000 and 2001, that the daily averaged opening and closing of the polynya follows a fortnightly cycle. Section 5 uses a combination of the ascending and descending swath Special Sensor Microwave Imager (SSM/I) data and AVHRR data to illustrate the diurnal polynya behavior, then compares the observations with numerical model results. Section 6 discusses the initial onset of the polynya in early winter, as shown from comparison of passive microwave and ScanSAR RADARSAT imagery. Section 7 provides a summary.

2. Numerical Model

[5] The study employs a coupled dynamic thermodynamic ice-ocean model. As described in detail by *Kowalik and Polyakov* [1999, Appendix], the ocean model is three-dimensional, baroclinic, Boussinesq, hydrostatic and nonlinear. It incorporates a turbulent closure model, which follows from the equation of turbulent kinetic energy and relates the eddy viscosity coefficient, the vertical shear of the horizontal velocity and the buoyancy. At the surface, the kinematic boundary condition for the vertical velocity allows for reproduction of surface gravity waves, including tidal waves. As *Polyakov et al.* [1998] describe in detail, an elastic-plastic constitutive law governs the ice dynamics. In this model, the ice thermodynamics apply individually to each of the following six ice thickness classes: 0.0–0.1 m, 0.1–0.3 m, 0.3–0.7 m, 0.7–1.2 m, 1.2–2.0 m, and >2 m. Each grid cell can contain all of the ice classes at different concentrations. The thermodynamic growth of each class within a grid cell depends on the atmospheric and oceanic heat fluxes, which differ because they depend on ice thickness. The classes interact when ridging occurs. In contrast, the ice dynamics and the ocean/ice stresses at each grid cell depend on the mean ice thickness and concentration of the different ice classes. For each grid point, the upper ocean temperature and salinity are defined as weighted averages of their respective water column properties. The horizontal resolution of the coupled model is 5.29 km; the vertical resolution has a variable grid spacing that over the summit of the bank equals 5 m. The time step is 9 s.

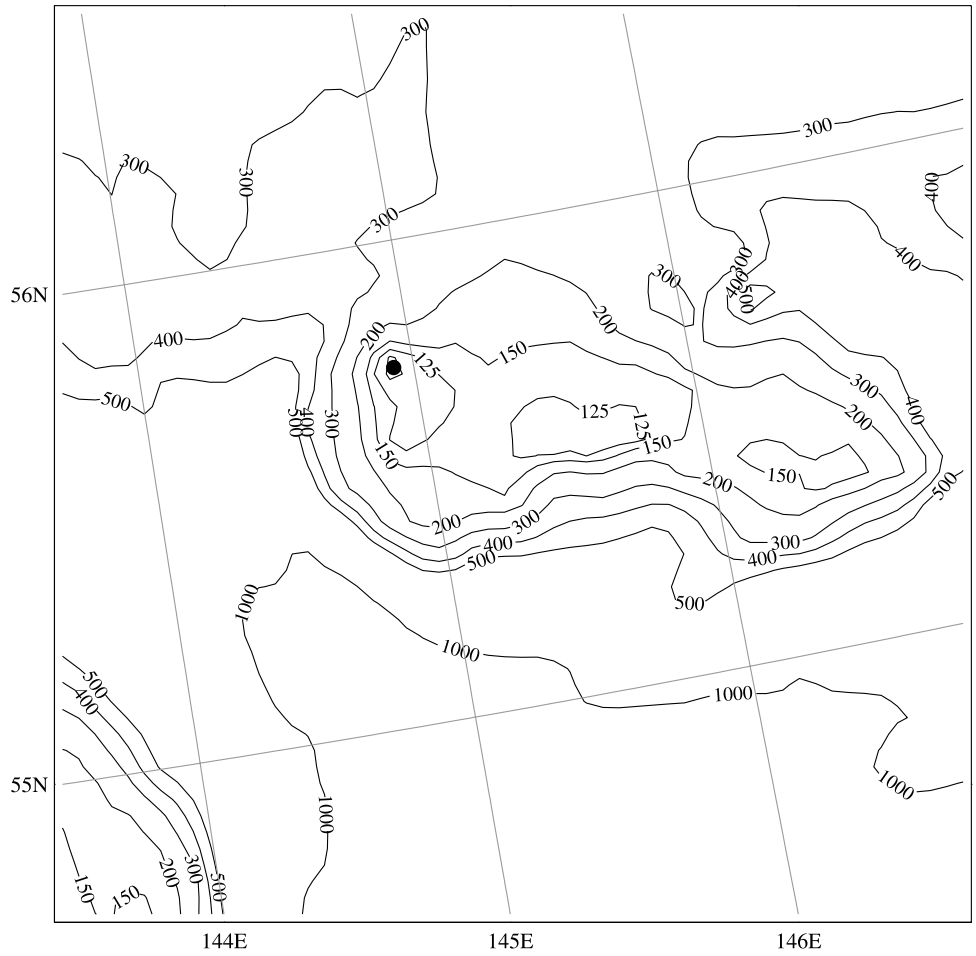

Figure 1b. Kashevarov Bank bathymetry, where the chart measures 175 km on a side. The black dot at the summit of the bank shows the location of the heat flux time series in Figure 2.

[6] The ice/ocean thermodynamic coupling depends on oceanic heat flux to the ice that in turn depends on the upper ocean vertical shear and buoyancy. As shown by *Kowalik and Polyakov* [1999, Figure 1] the model domain is restricted to the area around the bank. *Kowalik and Polyakov* [1999] and *Polyakov and Martin* [2000] use the same model and domain configuration. The model is forced by the diurnal barotropic K1 + O1 tides that are specified as sea level oscillations at the open boundaries, taken from *Kowalik and Polyakov* [1999]. The model is initialized with the temperature and salinity obtained from the summer numerical experiments of *Kowalik and Polyakov* [1998]. At the open boundary, the boundary conditions are as follows. For temperature and salinity, sponge boundary layers absorb the internal waves propagating toward the boundary. A gravity wave radiation boundary condition is specified for the cross-boundary velocity component, and a slip condition is specified for the along-boundary velocity component. A sponge condition is also specified for the ice velocity and the normal derivatives of the ice mass and concentration are set to zero. *Kowalik and Polyakov* [1999, section 4] compare the results of this model with 1996 summer-autumn tide gauge and current meter observations made on the bank [*Rogachev et al.*, 2001]. They find that although the model and observed K1 and O1 surface elevations agree to within 7%, for the same components, the model tidal current ellipses are about 30% smaller than the observed, in part because of the relatively poor 5-km spatial resolution.

[7] The current velocities and relative sea level heights are initially set equal to zero. Our justification for this initial condition is simple; from running the model, we find that after a period of 1 week to 10 days the tidal solution is sufficiently close to equilibrium for our purposes. In our case we have 50+ days of the model spin-up since the analysis described in section 5 applies to days 59 and greater. The model uses the monthly mean February values of air temperature, humidity, cloudiness and wind speed, equal respectively to $-14°C$, 80%, 0.6 and 10 m s^{-1}. Because of the small size of the bank, these parameters are assumed spatially constant. Given that the purpose of this study is to examine the specific effects of tides on the heat flux, ice drift and polynya formation, the model uses the climatic winds to compute the latent heat flux, but not to force an ice drift. The model integration begins with no ice, so that ice appears as a result of the surface water cooling and freezing. The mixed tides (K1 and O1) and ice dynamics and thermodynamics are computed for a 100-day period beginning on 1 January for both 2000 and 2001. The harmonic analysis of the computed time series at each point of the domain is used to separate the tidal constituents and to obtain its residual component.

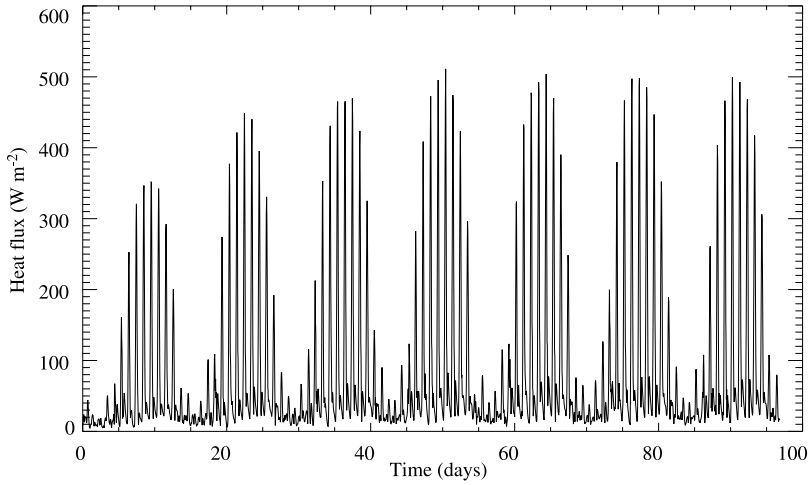

Figure 2. From the numerical model the tidally driven upwelling of heat over the western summit of the bank at the point marked by the dot in Figure 1b for days in 2000.

[8] For the year 2000, Figure 2 shows the strong heat flux from the ocean to the ice due to tidal mixing over the bank, at the point indicated by the black dot in Figure 1a. The figure shows that consistent with *Rogachev et al.* [2001], the heat flux has a strong diurnal signal that is made up of the K1 and O1 tidal oscillations and a fortnightly envelope. The nonlinear interaction of the diurnal constituents K1 and O1 generates a strong fortnightly tide with a period of 327.86 hr (13.66 days). The initial growth with time in the height of the fortnightly peak is the result of the model spin-up. After about 40 days, the figure shows that the fortnightly peaks have the same magnitude.

3. Evidence for Open Water Within the Polynya

[9] As observational evidence of open water within the polynya, Figure 3 shows two nearly coincident images of the polynya from day 65, 2000, which is near the peak in the fortnightly heat flux shown in Figure 2. The upper image shows a RADARSAT ScanSAR backscatter image taken at 2049 UTC, the lower image shows the ice surface temperature derived from AVHRR bands 4 and 5 and taken 32 min earlier at 2017 UTC. The ice surface temperature is derived using the algorithm of *Key and Haefliger* [1992] and *Key et al.* [1997]. From NCEP data for day 66 at 00 UTC, the 2-m air temperature is -15.8°C; the wind speed is 7.4 m s^{-1}. The AVHRR image shows that the polynya consists of relatively warm regions of what we assume is open water surrounded by colder thick ice, with a few cloud streaks extending to the southeast.

[10] The AVHRR image, however, does not permit an unambiguous identification of open water within the polynya. Because of the large water vapor flux from the polynya and its effect on the emitted radiances, the polynya surface temperatures in all of our AVHRR imagery are below the freezing point. From *Rogachev et al.* [2001], the surface salinity above the bank is 33.1 psu, corresponding to a freezing temperature of -1.81°C. In Figure 3b, there are 93 pixels with a surface temperature between -2° and -3°C, where only one pixel exists at the maximum observed temperature of -2°C. This pixel is located in the upwind part of the polynya where the effect of atmospheric water vapor would be minimized. These cold surface temperatures mean that the AVHRR image cannot be used as evidence of open water within the polynya.

[11] In contrast, the synthetic aperture radar (SAR) image shows that the region over the bank is composed of a combination of large floes separated by regions of bright return. If the water within the polynya were open, winds of 7 m s^{-1} would generate short Bragg scattering waves. Alternatively, if the surface water temperature is below freezing, then as *Wadhams and Holt* [1991] show, the grease ice formation would damp out the Bragg scattering waves, so that the bright regions in the image would appear dark and nonreflective. Comparison of the two images shows that the bright regions in the SAR are warm in the AVHRR image. This strongly suggests that the bright regions consist of open water at temperatures above freezing. The RADARSAT image thus provides direct evidence of open water within the polynya.

4. Fortnightly Modulation

[12] As evidence for the fortnightly cycle, Figure 4 shows for the 2000 and 2001 winters, daily averaged passive microwave imagery of the ice types over Kashevarov Bank. The images are derived from the Polynya Signature Simulation Method (PSSM) [*Markus and Burns*, 1995]. The PSSM works by applying the SSM/I 37- and 85-GHz data in succession, to (a) reduce the effect of clouds on the retrieval and (b) take advantage of the high spatial resolution 85-GHz data. By also utilizing the SSM/I antenna patterns, the resultant maps have a pixel size of 6.25 × 6.25 km^2. The PSSM is a classification algorithm. This means that for each pixel and depending on the range of brightness temperatures, the pixel is assigned to one of three classes, open water (OW), thin ice (THIN) and first year ice (FY).

[13] From comparison of their algorithm with an AVHRR Antarctic polynya image, *Markus and Burns* [1995, p. 4482] find that the thin ice category has a thickness of about 7 cm. The accuracy of this thickness depends on the AVHRR surface temperature and on the atmospheric heat flux calculation. Both of these are sensitive to errors in the

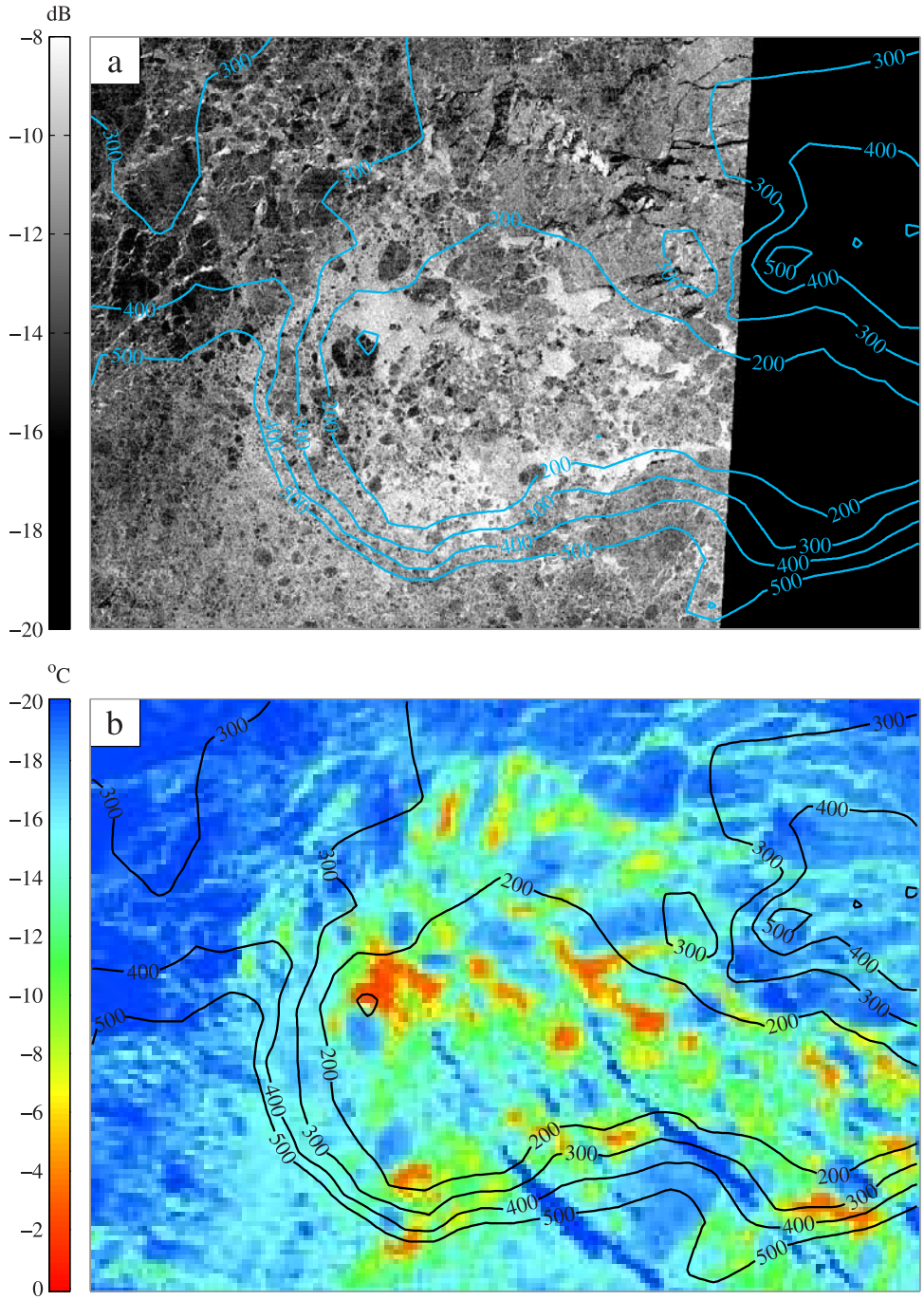

Figure 3. Images of the Kashevarov polynya for day 65, 2000. (a) A RADARSAT ScanSAR image acquired at 2049 UTC and (b) a surface temperature image derived from AVHRR acquired at 2017 UTC. The bottom topography is superimposed on both images. See text for further description.

meteorological observations and to surface conditions such as ice fog. This means that the AVHRR polynya area has large error bars so that the accuracy of the PSSM algorithm is difficult to establish. *Markus and Burns* [1995] show that the AVHRR- and PSSM-derived polynya areas qualitatively agree, and depending on the accuracy of the heat flux calculation and the weather observations, quantitatively agree to within about a factor of 2. To demonstrate that their algorithm is independent of cloud cover, they compare their polynya retrieval on two successive days, one cloud-covered and one cloud-free, and find that the two polynya areas agree within 4%. This suggests that their technique removes the 85-GHz sensitivity to clouds. For the same algorithm, *Hunewinkel et al.* [1998] use an atmospheric radiative transfer model and simulated brightness temperatures also to show that the algorithm is insensitive to clouds.

[14] On the figure, each square measures 175 km on a side, corresponding in shape and location to the Kashevarov chart in Figure 1b. In each row, the 14 images approxi-

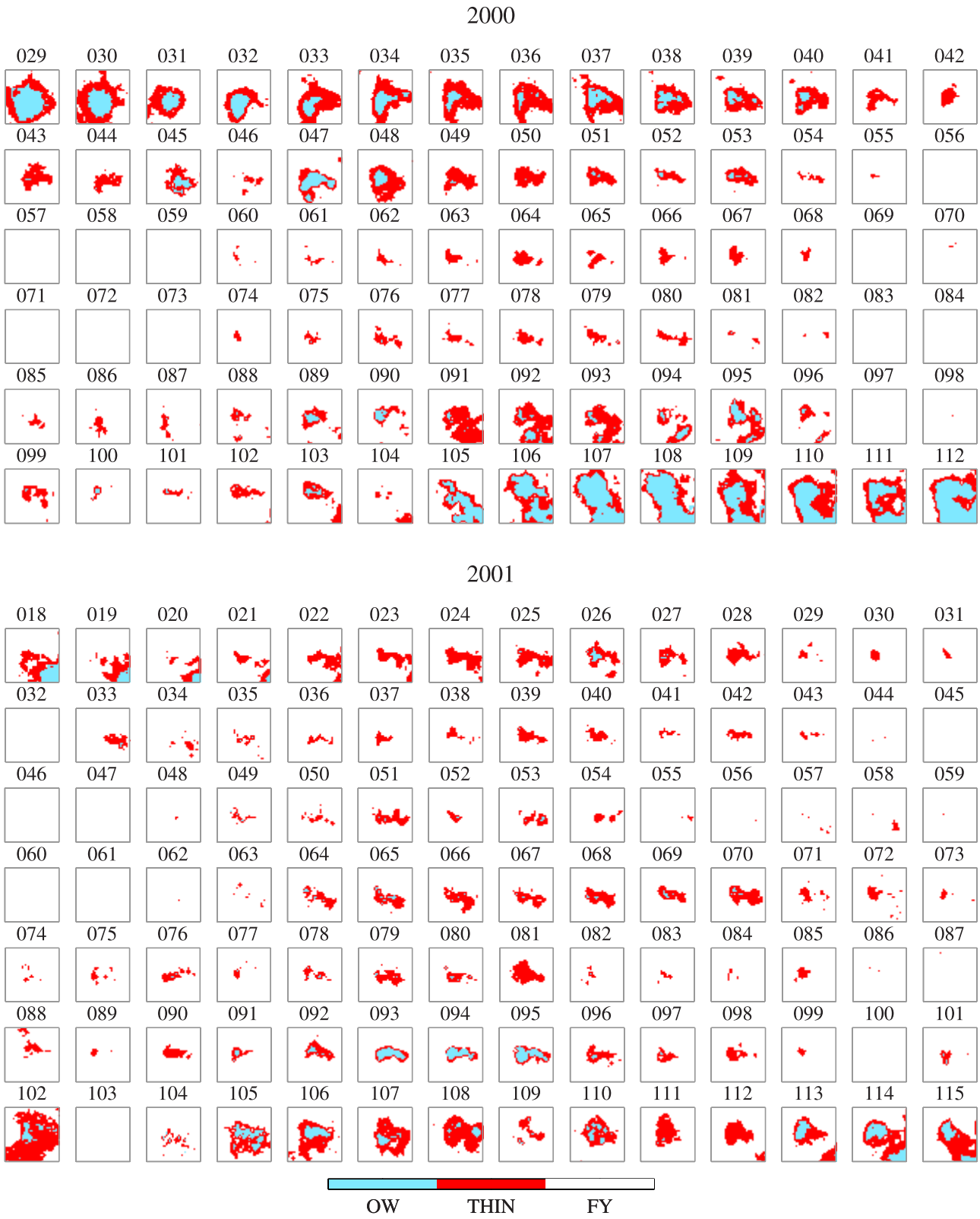

Figure 4. The daily averaged time series of the opening and closing of the Kashevarov polynya for the 2000 and 2001 winters, as derived from PSSM data. Each individual image measures 175 km on a side, exactly matching the chart area shown in Figure 1b. On the figure, white is first year (FY) ice, red is thin (THIN), and blue is open water (OW). The numbers above each image are the day numbers for the respective year, where day 1 is 1 January.

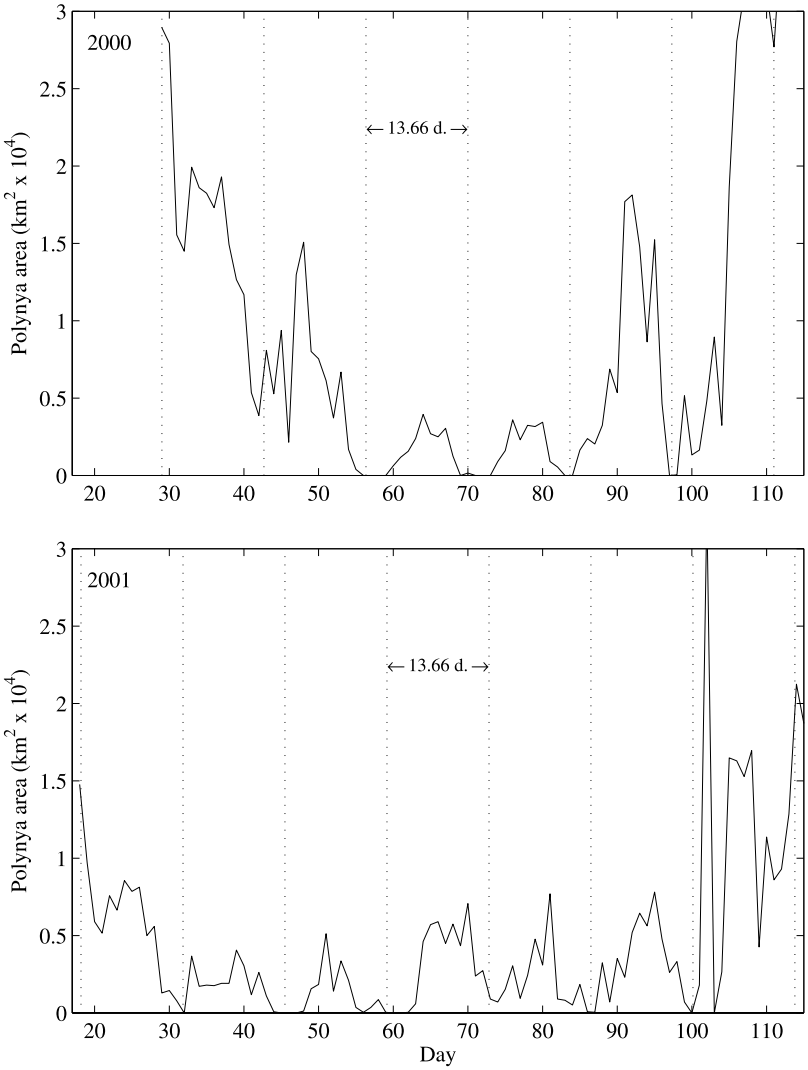

Figure 5. The daily averaged sum of the areas of open water and thin ice plotted versus time for 2000 and 2001, for the same data shown in Figure 4. The vertical lines correspond to the times of the maximum lunar declination or to the minima in the predicted fortnightly heat flux.

mately correspond to the 13.66-day fortnightly period. The left and right hand side of each row is aligned with the minima in the heat flux, which occurs at the maximum lunar declination [*Rogachev et al.*, 2001]; the maximum occurs about seven days later. The day number is written above each box, where for each year, day 1 corresponds to 1 January. Examination of the midwinter meteorological data shows that the atmospheric heat flux is strongly negative, so that in the daily average, the polynya size is determined by a balance between the upward oceanic heat flux, which tends to melt and thin the ice, and the atmospheric flux, which generates new ice growth. This balance is invalid in early winter, when the seawater temperature is above freezing, and in spring, when the atmospheric flux goes to zero or becomes positive.

[15] The upper set of images in Figure 4 show the polynya behavior for the year 2000 and extends from day 29 through day 112. The first row shows that the initial freeze-up of the polynya occurs approximately between days 29 and 42. Then beginning on about day 43 and continuing through day 98, or for the next four rows, the figure shows a periodic fortnightly growth and decay of the polynya, where the maximum polynya openings occur in the center of each row. Following day 99, spring warming becomes important and the polynya grows beyond the box boundaries. For 2001, the images show a similar cycle of opening and closing, although with more noise, occurring between days 32 and 101, following which time the polynya grows outside the box.

[16] For the same years and from the data shown in Figure 4, Figure 5 plots the sum of the polynya thin ice and open water area versus time. On each figure, the vertical dashed lines show the location of the minima in the heat flux that corresponds to the time of maximum lunar declination, again separated by 13.66 days. For 2000, the upper figure clearly shows that for the four cycles between days 40 and 98, the polynya area has a fortnightly component with its minima and maxima as predicted. For 2001, there are five cycles between days 30 and 100, with a similar pattern. For each year, following these periods, the atmospheric

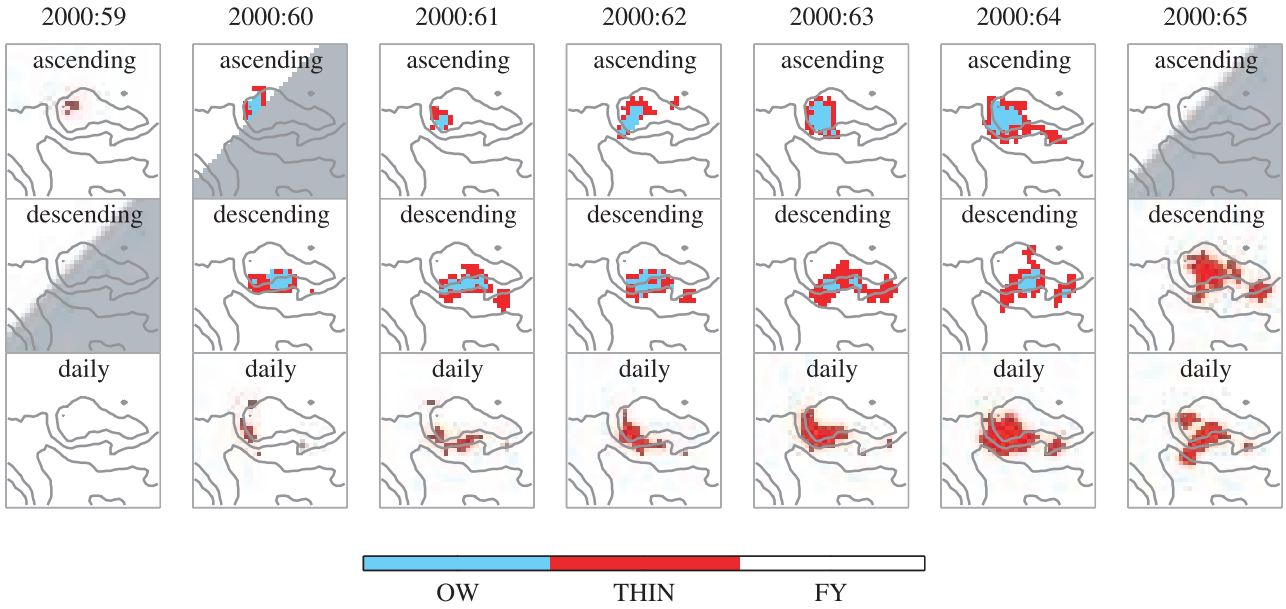

Figure 6. The diurnal polynya behavior for days 59–65, 2000, from PSSM data classified in an identical manner to Figure 4. Gray is missing data. The upper row shows the ascending swath data at approximately 0700 UTC, the middle row shows the descending swath data at approximately 2100 UTC, and the bottom row shows the daily averaged data. See text for further description.

temperatures rise about freezing and the polynya loses its identity. These data support the fortnightly variability in the daily averaged polynya area.

5. Diurnal Modulation

[17] The previous section uses daily averaged passive microwave data to examine the fortnightly variability of the polynya area. To examine the diurnal dependence, we use a combination of ascending and descending passive microwave swath data and AVHRR data, which are then compared with the numerical model results.

[18] Because of the SSM/I and AVHRR satellite orbits used in this analysis, coverage of the polynya tends to be concentrated in the early morning and early evening UTC. We begin with the passive microwave SSM/I swath data, which is taken from the DMSP satellite. The DMSP is in a dawn-dusk orbit, with approximate equator crossing times of 0600 local time for the descending passes and 1800 for the ascending. Within the Okhotsk, the bank is covered by either one or two successive passes, which take place at approximately 0700 UTC (ascending) and 2100 UTC (descending), respectively corresponding to local afternoon and morning. The reason that these times are separated by 14 hours instead of 12 hours is due to the northern location of the Okhotsk Sea and to the difference between the overpass times of the ascending and descending orbits. For days 59–65, Figure 6 shows the PSSM analysis of the SSM/I data, classified in an identical manner to Figure 5. The three rows respectively show the ascending and descending swath data and its daily average. For times greater than day 65, our examination of similar PSSM imagery that is not included here shows that this shift in polynya shape and position recurs at the fortnightly period, so that the sequence in Figure 6 is typical of the midwinter behavior.

[19] The first row shows the ascending swath imagery taken at about 0700 UTC. These images show that the polynya forms over the western edge of the bank, then increases in area with time. In contrast, the second row shows that for the descending swath images at 2100 UTC, the polynya forms over the southwest edge of the bank, spreads laterally to the east through about day 63, then appears to spread randomly across the bank. Comparison of the ascending and descending imagery shows that between 0700 and 2100 UTC, the polynya shifts from a location over the western rise in the ascending pass, to a location over the southern edge of the bank in the descending pass where the polynya becomes elongated in the east-west direction. Also, beginning on day 60, the ascending and descending polynyas contain both open water and thin ice.

[20] The third row shows the daily averaged polynya images. Unlike the ascending and descending images, these consist only of thin ice. This difference between the swath and average images is due to the shift in polynya location with the diurnal cycle. This shift means that the regions of open water do not necessarily overlap between the ascending and descending swaths, so that the daily averaged polynya consists of thicker ice than the swath images. Examination of the average images also shows that they do not always appear to be the sum of the ascending and descending images. The reason for this depends on the nature of the PSSM classification algorithm. If for the same pixel, the PSSM classifies ice from the morning overpass as thin ice and from the evening overpass as thick first year ice, their daily average can only be one of these two categories. If for example, the thin ice is close to being classified as thick ice, it is more likely that the average will be thick ice.

[21] The AVHRR images exhibit a similar diurnal behavior. For the clear days 61–64, Figure 7 shows AVHRR imagery of the polynya with the topography superimposed.

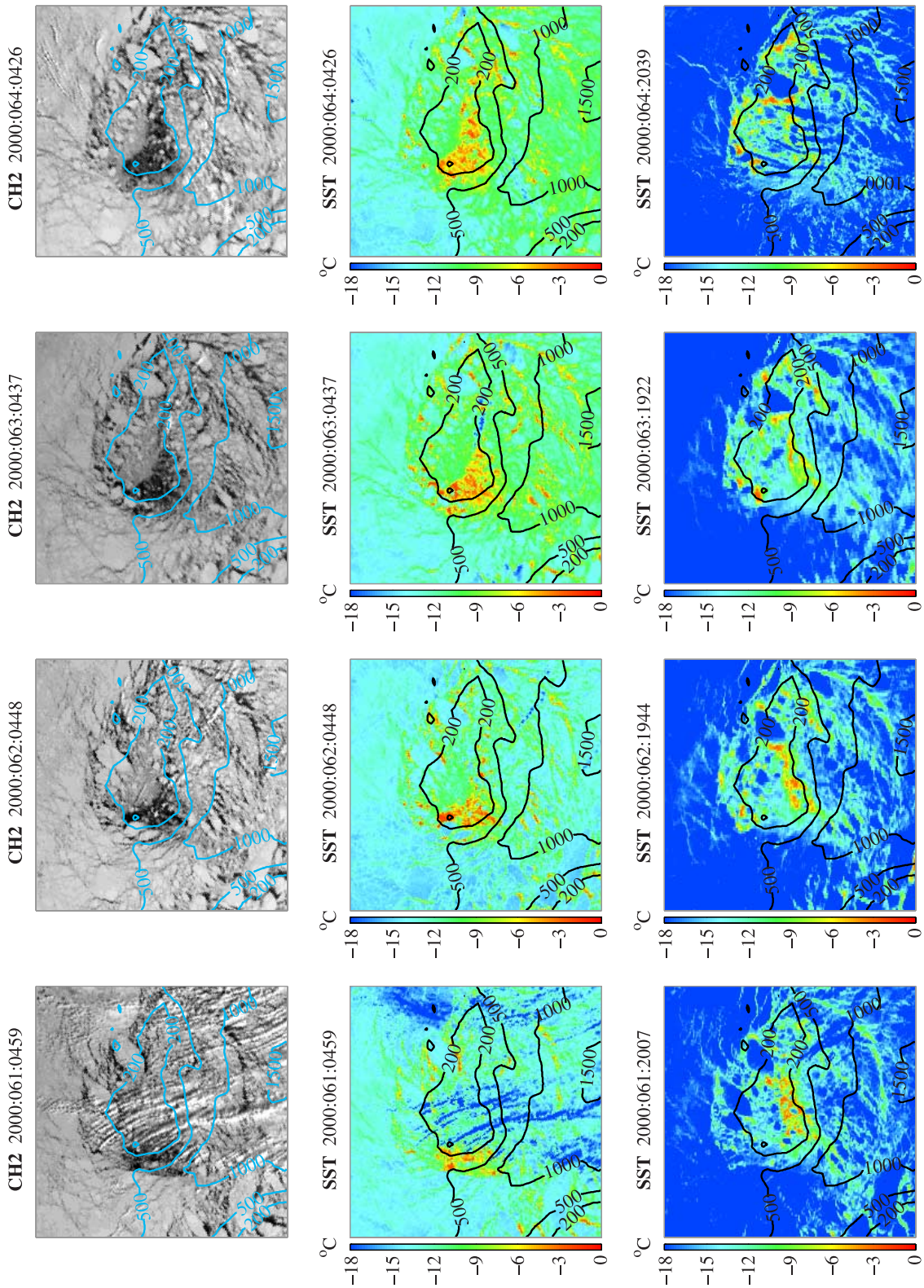

Figure 7. The diurnal polynya behavior for days 61–64, 2000, from AVHRR infrared imagery. The topography is shown on each image. The upper two rows show the 0430 UTC near-infrared and SST imagery; the bottom row shows the 2000 UTC surface temperature image. See text for further description.

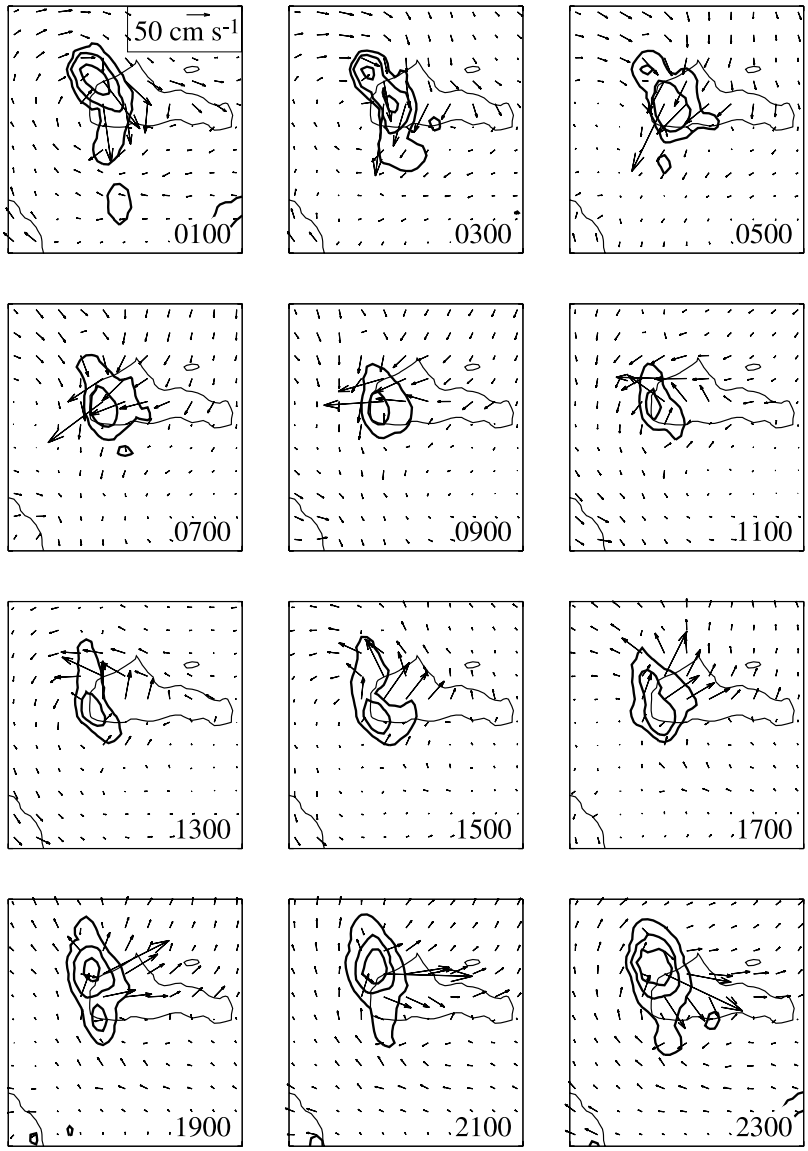

Figure 8. The numerically derived heat flux behavior compared with the tidal currents at 2-hour intervals for day 63, 2000, and beginning at 0100 UTC. The dark lines show the heat flux contours, the light lines show the bathymetry, and the arrows show the tidal currents. Proceeding from the outside in, the heat flux contours correspond to 50, 100, and 150 W m^{-2}.

The upper two rows of figures show near-infrared and infrared imagery taken at about 0430 UTC, corresponding to local afternoon in the Okhotsk. The top row shows the near-infrared (channel 2 or 0.725–1.0 μm), which gives better open water/sea ice contrast than the visible channel 1; the middle row shows the ice and water surface temperature, again from the infrared channels 4 and 5 using the Key et al. algorithm described above. *Rogachev et al.* [2001] also show two of these images. On the near-infrared images, ice is white, open water and thin ice are dark, and clouds are visible as white streaks. On the corresponding temperature images, ice is cold, the cloud streaks are very cold, and open water and thin ice are warm. The bottom row shows the infrared surface temperatures at about 2000 UTC; because these images were acquired in the local early morning when the sun is below the horizon, there is no concurrent visible imagery. Examination of the upper two rows of images, which were acquired at approximately the same time as the ascending SSM/I data, show that similar to the PSSM, the polynya is initially centered over the western rise, then grows with time to the east along the southern edge of the bank. In contrast, the lower row, which was acquired at approximately the same time as the descending SSM/I data, shows that through day 62 or 63, the polynya is initially located along the southern edge, following which time it spreads almost randomly to other locations. None of our satellites provided data in the local noon timeframe.

[22] The numerical modeling results are similar to the satellite observations. We present these results in three ways; the first and second respectively show at 2-hour intervals throughout a single day, the location of the maximum heat flux over the bank and the polynya size and location; the third shows the polynya behavior over

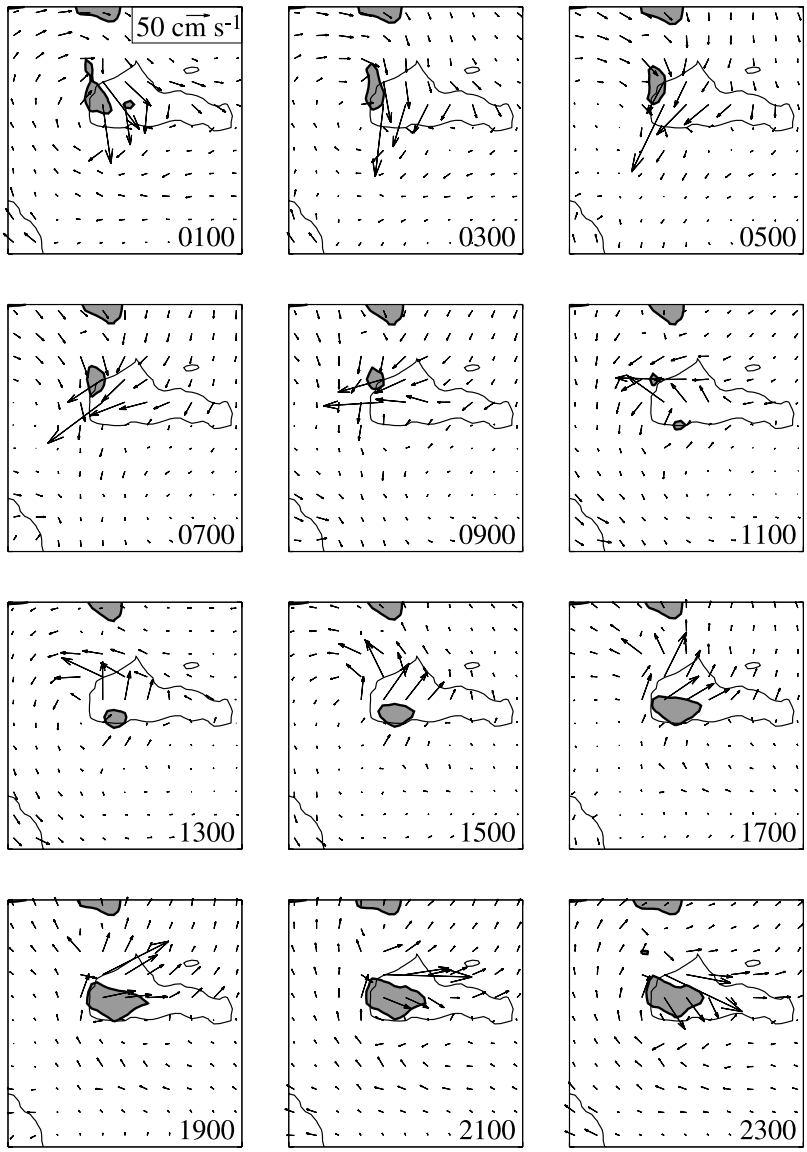

Figure 9. The numerically derived ice behavior compared with the tidal currents at 2-hour intervals for day 63, 2000. The shaded area shows the 25% ice concentration regions, with the bathymetry and tidal currents as described on Figure 8.

several days at the times of the ascending and descending passes, and for the daily average. For the first case, on day 63 and beginning at 0100 UTC, Figure 8 shows the location of the heat flux contours with the tidal currents superimposed; for the second case, Figure 9 shows the location of the contour within which ice thicknesses greater than 0.1 m occupy no more than 25% of the area, also with tidal currents superimposed. Examination of Figure 8 shows that the location of the maximum heat flux is initially in the north, moves south and east with the tidal currents, then returns to the north. The heat flux has a maximum at 0100 UTC and again at about 2300 UTC, and a minimum at 1100 UTC. The position and magnitude of the maximum heat flux is strictly determined by the tidal currents and mixing, and is independent of the ice cover properties.

[23] In contrast, Figure 9 shows that the polynya size and position are determined by two factors, the magnitude and position of the heat flux maximum, and tidal advection of the ice cover. Advection can bring thicker ice over the region of maximum upwelling, or translate the polynya away from the region of maximum flux. This makes it difficult to separate the effects of tidal advection and heat flux on the polynya position. Comparison of Figures 8 and 9 shows that the polynya size is approximately in phase with the heat flux, having its minimum at about 1100 UTC and its maximum between 1900 and 2300 UTC. Figure 9 also shows that from about 1300 to 2300 UTC and consistent with the tidal currents, the polynya becomes elongated in the east-west direction with its location offset from that of the heat flux maximum.

[24] Third, Figure 10 shows the polynya behavior for days 59–65, 2000. On this figure, the first and second rows show the location of the 25% ice contour at 0700 and 2100 UTC, approximately corresponding to the image times in Figures 6 and 7; the third row shows the daily average. Examination of the 0700 UTC model results shows that the

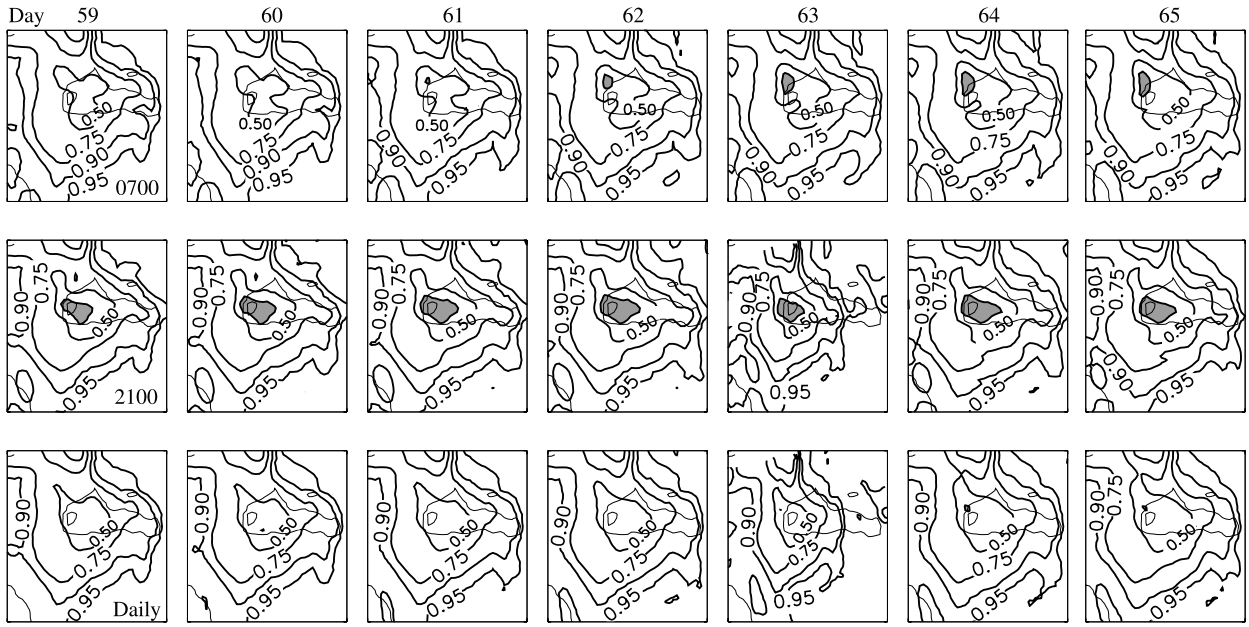

Figure 10. The numerically derived ice concentrations over the bank for days 59–64, 2000, at 0700 and 2100 UTC and for the daily average. On each image the heavy solid lines are contours of ice concentration at intervals of 0.95, 0.90, 0.75, 0.50, and 0.25, where the area covered by concentrations less than 0.25 are shaded gray. The light solid lines show the bottom contours.

polynya is initially located over the western rise, where it grows in size with time. In contrast, the 2100 UTC results show that the 25% contour is shifted to the south and tends to be larger and elongated in the east-west direction. For the daily average, the third row of Figure 10 shows that because of the oscillations in the polynya position, the 25% contour does not appear until day 63 or 64, and occupies a very small area. This behavior is consistent with Figure 6, which shows that the daily averaged PSSM polynyas consist of thicker ice than the instantaneous swath images.

[25] Comparison of Figure 10 with Figures 6 and 7 shows that the model and observations exhibit many of the same features. The size of the model and observed polynyas increase with time, and the 0700 UTC polynya tends to be smaller than the 2100 UTC polynya. Unlike the observed polynya however, the 0700 UTC model polynya is displaced to the north, and does not become elongated with time along the southern edge of the bank. At 2100 UTC, both the model and observed polynyas have an east-west orientation, although the model polynya is again displaced slightly to the north. The disagreements between the model results and the observations may occur because of inadequate physics in the model, the relatively large 5.4-km grid spacing, or because of inaccuracies in the observed topography. Even with the differences, both the images and the model support the diurnal shift in the location and shape of the low ice concentration region.

6. Early Winter Onset of the Polynya

[26] We next examine two images that illustrate the polynya onset in early winter. For 24 January 2000, Figure 11 shows a PSSM image of the ice distribution in the Okhotsk. For this day, the wind velocity is about 10 m s^{-1} from the northwest; the air temperature is about −25°C. The image acquisition date is slightly past the peak in the fortnightly upwelling; the black rectangle outlines the Kashevarov Bank. Examination of the image shows that open water extends from the east into the ice cover and over the bank. From Figure 4, as time goes on, pack ice completely surrounds the polynya. This formation of the polynya from an initial embayment of ice recurs during heavy ice years. It also occurs in the formation of the Cosmonaut polynya in the Southern Ocean [*Comiso and Gordon*, 1987, 1996, Plate 2, 20–27 July].

[27] During the periods of strong northerly winds that are common in winter, ice is advected into the polynya from the north and away from the polynya to the south, so that the ice embayment is not static. Because of the recurrence of this embayment from year to year, it is appropriate to examine the details of the accompanying ice processes. For this purpose, Figure 12 shows a RADARSAT ScanSAR image taken at 2045 UTC on the same day with its boundaries corresponding to the black outlined rectangle in Figure 11, and Figure 13 is a cartoon of the ice and inferred water structure along a transect running north/south across the bank. Unfortunately, examination of concurrent AVHRR data shows that this day is cloudy, so that we lack supporting AVHRR imagery.

[28] On Figure 12, the irregular white lines show the bottom topography; at the bottom left, the northern tip of Sakhalin Island is just visible. The dependence of the radar backscatter on look angle creates the increase in image brightness to the right. The black and white dashed line shows the location of the boundary between the thin ice and open water in Figure 11. Examination of this line shows that

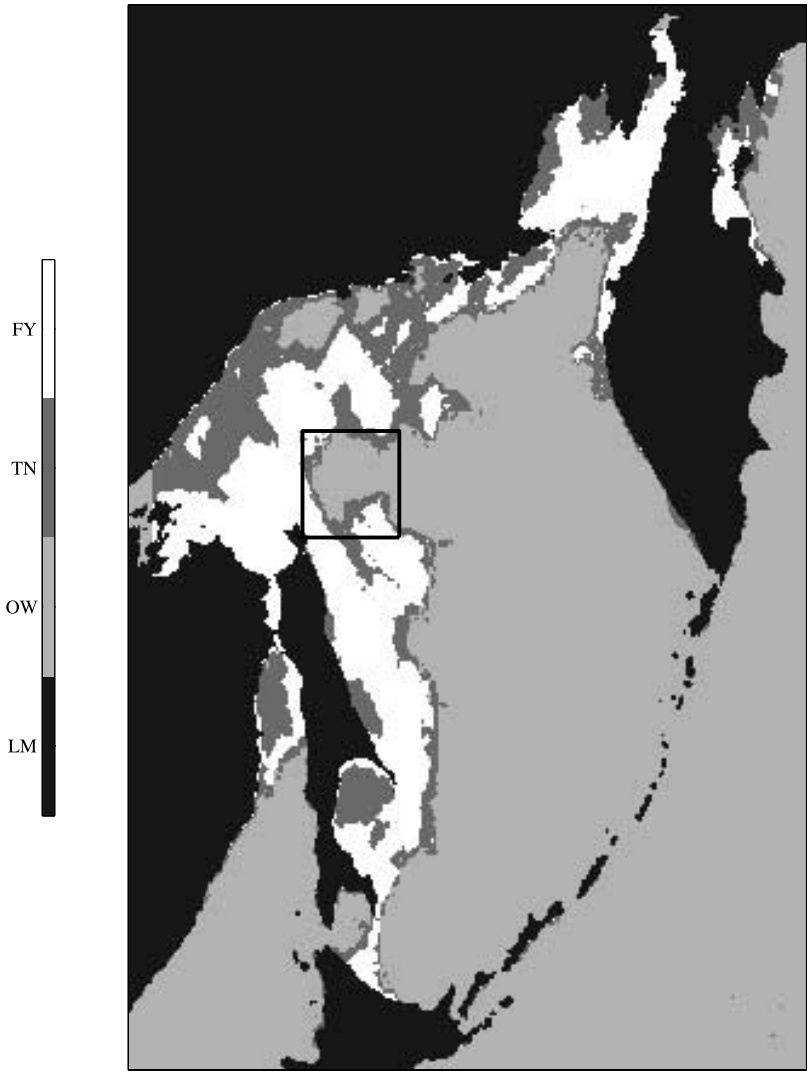

Figure 11. A PSSM daily averaged image of the Okhotsk sea ice concentration for day 24, 2000. Land is black, white is first year ice, dark gray is thin ice, and light gray is open water. The black outlined rectangle is over the Kashevarov Bank and shows the ScanSAR coverage given in Figure 12. The wind velocity is about 10 m s^{-1} from the northwest; the 2-m air temperature is about −25°C.

except to the southeast, the PSSM boundary approximately corresponds to the boundary between open water and thin ice shown in the SAR image. The ice behavior within the three white-outlined square boxes labeled (a), (b), (c) illustrate the different kinds of ice behavior in the vicinity of the bank. Box (a) shows the region over and to the north of the bank. Within this box, and just south of the northern 200-m contour, the most prominent feature is a fishhook-shaped band of ice labeled 'F' that protrudes from the east into the open water over the bank. Similar narrow bands of ice are visible just north of this box. From a field study at the Bering Sea ice edge, *Martin et al.* [1983] show that such bands are caused by a combination of off-ice winds, wave fracture of large floes into small floes, and surface water temperatures above freezing. These conditions erode irregularly shaped ice features into the long linear bands associated with wind waves and above-freezing water temperatures. Their presence suggests that as expected, the water temperature over the bank is above freezing.

[29] Box (b) shows the region south of the bank where upwelling is negligible. In this box and primarily south of the 1000-m-depth contour, there is a transition from relatively bright open water to a very dark nonreflective surface. We assume that this bright-to-dark transition occurs for the following reason. Over the bank, the heat flux from below exceeds the atmospheric heat loss. Therefore, as we move south and off the bank to a region where upwelling is unimportant, the atmospheric heat loss will exceed the upwelled heat flux. Also, because of the strong northerly winds, within the open water over the bank, wind waves and swell increase in amplitude and wavelength in the southerly direction. The combination of these factors means that moving to the south, at some location the temperature of the wave-agitated surface waters must reach the freezing point. At this location, and because of the wind waves, ice formation occurs in the form of frazil and grease ice. As *Wadhams and Holt* [1991] show, grease ice damps out the short Bragg-scattering waves and creates the dark

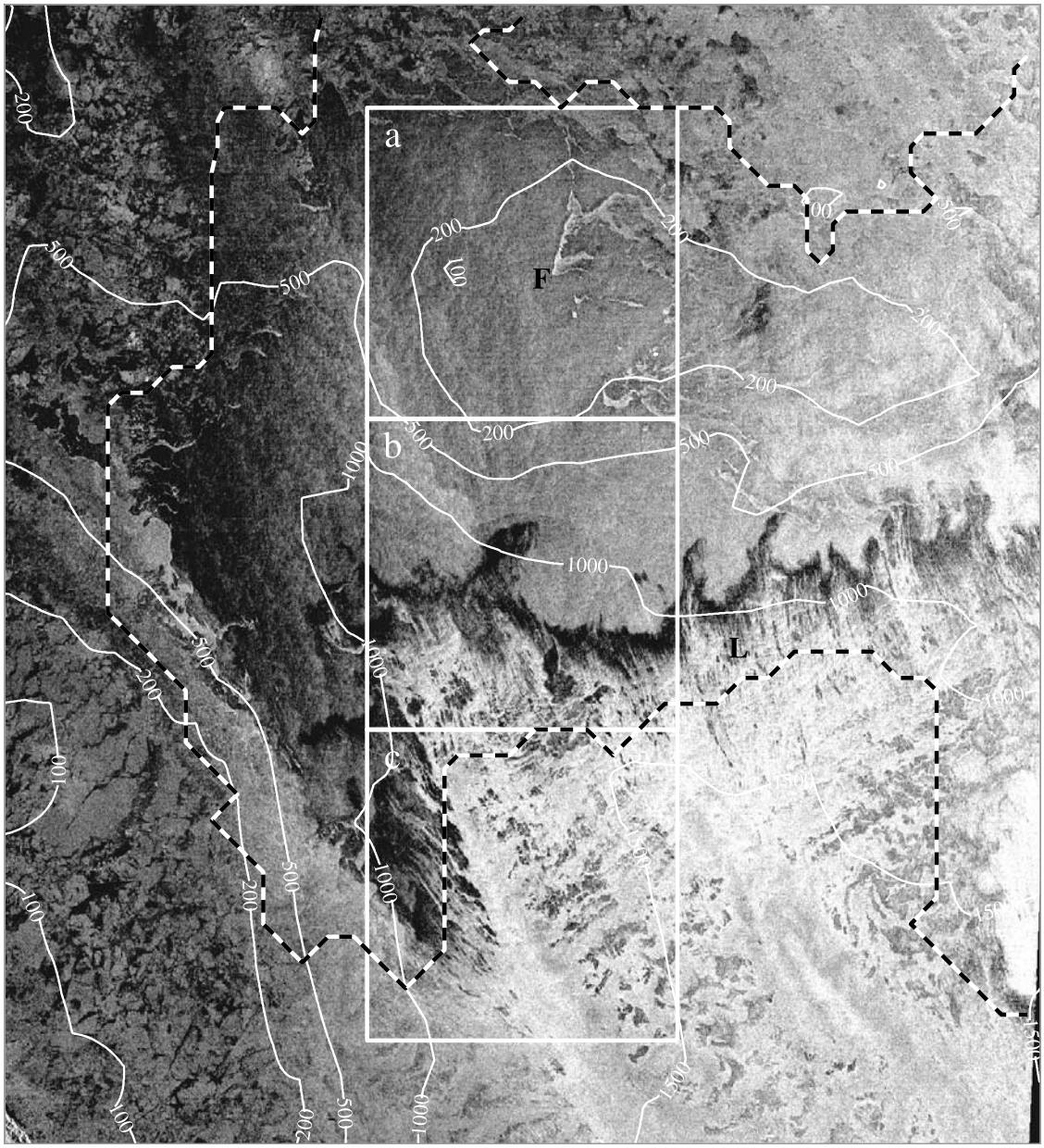

Figure 12. A RADARSAT ScanSAR image of the area within the black outlined rectangle shown in Figure 11 for the same day at 2045 UTC. The northern tip of Sakhalin Island is visible at the bottom left. The irregular white lines show the bottom topography. The three white squares aligned in the vertical and labeled a, b, and c measure 75 $\times$ 75 km^2. The white and black dashed line shows the boundary between open water and thin ice given in Figure 11. The features labeled F and L are described in the text.

nonreflective surface observed in the image. Thus the northern boundary of the dark area marks the point south of the bank where the surface water first reaches the freezing temperature, yielding the formation of a thin grease ice layer. The grease ice also marks the geographic boundary between the region where the ice floes melt, creating a freshening of the surface waters, to the region where freezing occurs, creating ice growth and salt rejection.

[30] Proceeding south of the nonreflective region in Box (b), a linear series of bright lines running approximately north/south grow out of the dark grease ice. As illustrated by the many SAR images of *Drucker et al.* [2003], these bright lines are approximately parallel to the wind direction and indicate the formation of Langmuir plumes. To the right of Box (b), similar plumes are labeled 'L'. These plumes are bright because of either the presence of pancake ice in the plumes, where the raised pancake rims generate Bragg scattering, or because of Bragg scattering from the waves in the open water separating the plumes. Because of the cooling, salt rejection and mixing associated with the ice formation and Langmuir circulation, Figure 13 shows that the depth where the water is at its freezing point T_f and the corresponding mixed layer depth increase with distance away from the bank. The image also shows that further downwind, the plumes grow together to form a nearly solid and very bright collection of floes. The growth of the

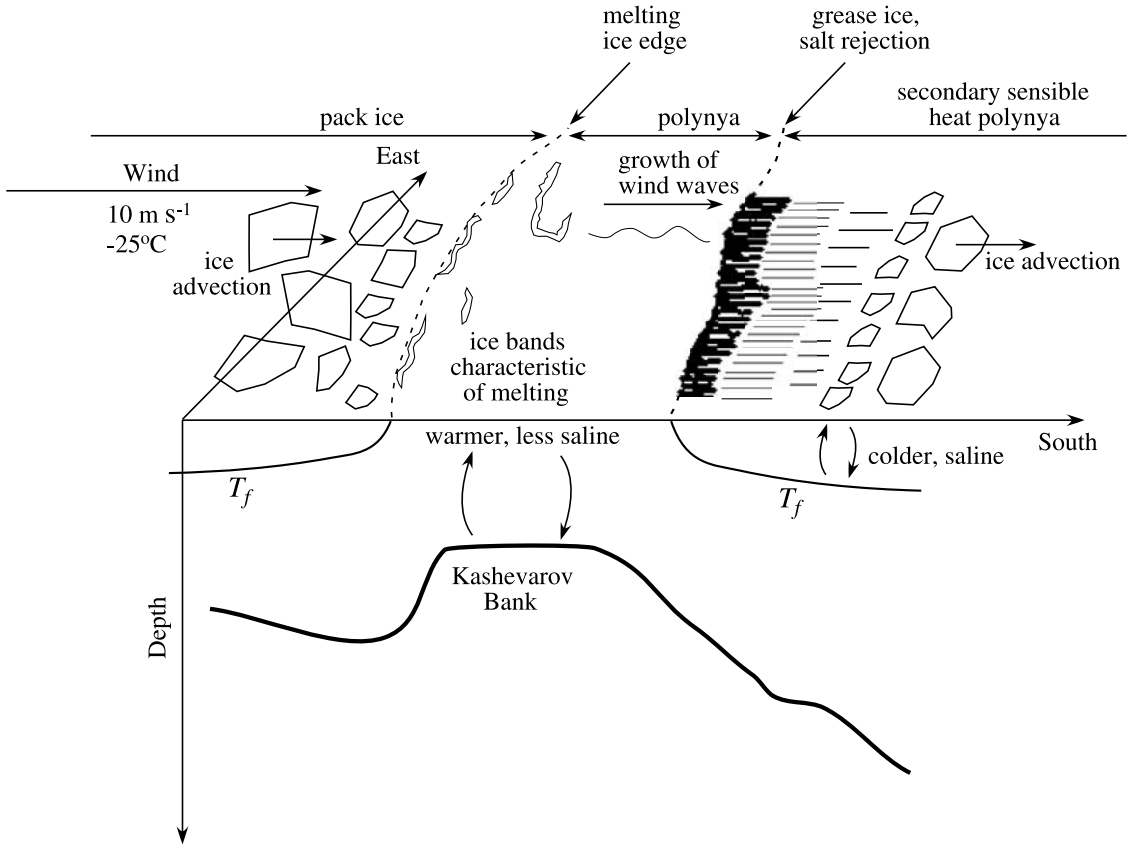

Figure 13. A cartoon of the ice and inferred water features shown in Figure 12 along a transect running north-to-south across the summit of the bank. North is to the left, south to the right, and the arrow indicates the wind direction. See text for further description.

plumes and the accompanying salt rejection suggest that the halocline depth also increases with distance downwind. Further south, in box (c), the ice surface becomes irregular but remains bright.

[31] In summary, the image suggests that in early winter, the Kashevarov polynya consists of two parts, an upwelling polynya over the bank and a secondary polynya downwind of the bank with properties similar to coastal polynyas. In this case, the transition to freezing serves as the coast, and the halocline depth acts as the ocean bottom. Although the formation of wind waves and swell in the open water area over the bank means that the secondary polynya differs from a true coastal polynya, the imagery suggests that in the early stages of the formation of mid-ocean polynyas, their downwind regions serve as oceanic salt sources. Thus during early winter, the Kashevarov Bank region is characterized by a two part polynya, a warm upwelling region over the bank and a secondary freezing region south of the bank.

7. Summary

[32] The paper compares the time series of polynya formation over the Kashevarov Bank derived from a numerical model with that observed from passive microwave, SAR and AVHRR imagery. Evidence of open water within the polynya is presented in the form of the backscatter distribution within a ScanSAR image, which is consistent with the presence of a mixture of floes and open water over the bank. The numerical model shows that over the bank, the heat flux and polynya area exhibit fortnightly and diurnal cycles. Daily averaged passive microwave imagery of the polynya opening and closing also exhibits a strong fortnightly cycle, consistent with the model. The model also shows a diurnal oscillation in the position of the maximum heat flux and of the polynya over the bank. Examination of ascending and descending SSM/I imagery and of AVHRR imagery shows similar diurnal changes in the polynya position. Finally, the paper compares a passive microwave and ScanSAR image of the polynya onset. The comparison shows that under conditions of cold strong winds, the effect of the upwelling is to generate melting at the upwind edge of the bank, a polynya over the bank and a secondary freezing polynya downwind of the bank. This secondary polynya resembles a coastal polynya in that it adds salt to and extracts heat from the water column. Similar secondary polynyas may also occur in other mid-ocean polynyas such as the Cosmonaut polynya in the Antarctic Ocean.

[33] **Acknowledgments.** SM and RD gratefully acknowledge the support of NSF under grant number OCE-9811097, and of NASA under grant number NAG5-11057. We also thank the Alaska SAR Facility and RADARSAT for acquiring the ScanSAR imagery used in the paper. We also acknowledge that the daily averaged SSM/I data in the polar stereographic grid and the swath data in the EASE grid were obtained from the National Snow and Ice Data Center in Boulder, CO. IP thanks the Frontier Research System for Global Change for financial support.

References

Alfultis, M. A., and S. Martin (1987), Satellite passive microwave studies of the Sea of Okhotsk ice cover and its relations to oceanic processes, 1978–1982, *J. Geophys. Res.*, *92*, 13,013–13,028.

Comiso, J. C., and A. L. Gordon (1987), Recurring polynyas over the Cosmonaut Sea and the Maud Rise, *J. Geophys. Res.*, *92*, 2819–2834.

Comiso, J. C., and A. L. Gordon (1996), The Cosmonaut Polynya in the Southern Ocean: Structure and variability, *J. Geophys. Res.*, *101*, 18,297–19,313.

Drucker, R., S. Martin, and R. Moritz (2003), Observations of ice thickness and frazil ice in the St. Lawrence Island polynya from satellite imagery, upward looking sonar, and salinity/temperature moorings, *J. Geophys. Res.*, *108*(C5), 3149, doi:10.1029/2001JC001213.

Hunewinkel, T., T. Markus, and G. C. Heygster (1998), Improved determination of the ice edge with SSM/I data for small-scale analyses, *IEEE Trans. Geosci. Remote Sens.*, *36*, 1795–1808.

Key, J., and M. Haefliger (1992), Arctic ice surface temperature retrieval from AVHRR thermal channels, *J. Geophys. Res.*, *97*, 5885–5893.

Key, J., J. Collins, C. Fowler, and R. Stone (1997), High-latitude surface temperature estimates from thermal satellite data, *Remote Sens. Environ.*, *61*, 302–309.

Kowalik, Z., and I. Polyakov (1998), Tides in the Sea of Okhotsk, *J. Phys. Oceanogr.*, *28*, 1389–1409.

Kowalik, Z., and I. Polyakov (1999), Diurnal tides over Kashevarov Bank, Sea of Okhotsk, *J. Geophys. Res.*, *104*, 5361–5380.

Markus, T., and B. A. Burns (1995), A method to estimate subpixel-scale coastal polynyas with satellite passive microwave data, *J. Geophys. Res.*, *100*, 4473–4487.

Martin, S., P. Kauffman, and C. Parkinson (1983), The movement and decay of ice edge bands in the winter Bering Sea, *J. Geophys. Res.*, *88*, 2803–2812.

Polyakov, I., and S. Martin (2000), The interaction of the Okhotsk Sea diurnal tides with the Kashevarov Bank polynya, *J. Geophys. Res.*, *105*, 3281–3294.

Polyakov, I. V., I. Y. Kulakov, S. A. Kolesov, N. E. Dmitriev, R. S. Pritchard, D. Driver, and A. K. Naumov (1998), Coupled sea ice-ocean model of the Arctic Ocean, *J. Offshore Mech. Arct. Eng*, *120*, 77–84.

Rogachev, K. A., E. C. Carmack, A. S. Salomatin, and M. G. Alexanina (2001), Lunar fortnightly modulation of tidal mixing near Kashevarov Bank, Sea of Okhotsk, and its impacts on biota and sea ice, *Prog. Oceanogr.*, *49*, 373–390.

Wadhams, P., and B. Holt (1991), Waves in frazil and pancake ice and their detection in Seasat synthetic aperture radar imagery, *J. Geophys. Res.*, *96*, 8835–8852.

R. Drucker and S. Martin, School of Oceanography, University of Washington, Box 357940, Seattle, WA 98195–7940, USA. (seelye@ocean.washington.edu)

T. Markus, Laboratory for Hydrospheric Processes, NASA Goddard Space Flight Center, Greenbelt, MD 20771, USA.

I. Polyakov, International Arctic Research Center, University of Alaska Fairbanks, 930 Koyukuk Drive, Fairbanks, AK 99775, USA.